ACS Energy LETTERS

http://pubs.acs.org/journal/aelccp

Direct Membrane Deposition for CO_2 Electrolysis

Tartela Alkayyali,[⊥] Ali S. Zeraati,[⊥] Harrison Mar,[⊥] Fatemeh Arabyarmohammadi, Sepehr Saber, Rui K. Miao, Colin P. O'Brien, Hanshuo Liu, Zhong Xie, Guangyu Wang, Edward H. Sargent, Nana Zhao,* and David Sinton*

Cite This: *ACS Energy Lett.* 2023, 8, 4674−4683

Read Online

ACCESS | Metrics & More | Article Recommendations | Supporting Information

ABSTRACT: **The use of forward-bias bipolar membranes (f-BPM) in CO_2 electrolyzers offers the advantage of avoiding costly CO_2 reactant loss. However, current f-BPM-based electrolyzers require a high voltage and produce H_2 at the expense of CO_2 reduction products. In this work, we develop a direct membrane deposition (DMD) approach that combines anion and cation exchange membranes (AEM and CEM, respectively) to increase transport and facilitate CO_2 regeneration. The DMD approach provides flexibility to tune the properties of the composite and optimize the AEM:CEM ratio for low resistance and low H_2 evolution. Compared to a standard f-BPM, the DMD approach reduced the H_2 Faradaic efficiency by 2-fold (25% vs 12%, respectively), reduced mass transport resistance by over 50%, decreased full-cell potential by 0.84 V, increased the selectivity toward multicarbon products by over 2-fold (29% vs 65%, respectively), and achieved >17% in multicarbon product energy efficiency at 300 mA cm^{-2}.**

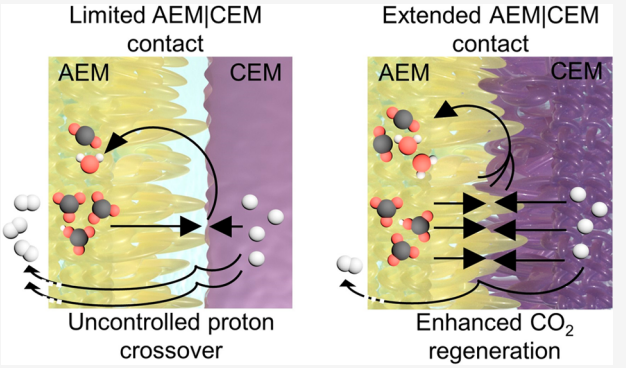

The electrocatalytic conversion of CO_2 to high-value, large-market products and feedstocks using renewable electricity offers a pathway to carbon neutrality. Electrocatalytic systems based on the membrane electrode assembly (MEA), or zero-gap, configuration offer stability and scalability beyond that of flow cell and H-cell systems.[1,2] However, CO_2 reduction reaction (CO_2RR) electrolyzers require advances in product selectivity (Faradaic efficiency, or FE), cell voltage, and single-pass conversion (SPC; the fraction of input CO_2 that is converted to CO_2RR products).[3,4]

CO_2RR electrolyzers commonly employ alkaline/neutral electrolytes, as multicarbon products (C_{2+}) are favored at high pH. However, reactant CO_2 is lost to (bi)carbonates under these conditions; the CO_2 crosses over to the anode in the form of HCO_3^- and CO_3^{2-} ions via the anion exchange membrane (AEM).[5] To address this challenge, alternative system configurations,[6] such as bipolar membranes (BPM) in forward-bias mode (f-BPM),[7] have been recently employed. When an AEM is placed facing the cathode, CO_2 regeneration can take place from the combination of (bi)carbonate ions and protons (provided by a cation exchange membrane (CEM)). The regenerated CO_2 then diffuses back to the cathode surface, where it can undergo further conversion into valuable products, resulting in notable SPCs (>70%).[7,8] However, these systems encounter several challenges, including high H_2 production (>20% FE), high cell potential (>4.3 V),[7,8] or low C_{2+} FE (<40%),[9] when operating at industrially relevant current densities (>200 mA cm^{-2}).

In an f-BPM, CO_2 regeneration occurs at the intersection of AEM and CEM polymer chains (i.e., the active AEM|CEM interface), at which (bi)carbonate ions from the cathode react with protons from the anode to form CO_2 and H_2O. The higher the rate of this regeneration reaction, the lower the rate of proton crossover from the anode to the cathode due to electromigration. Avoiding proton transport to the cathode reduces the H_2 evolution reaction (HER)[10] that competes with CO_2RR. We postulated that the high H_2 FE commonly observed in f-BPM systems may arise due to voids that result when an AEM material is sprayed onto the cathode and sandwiched with a commercial standalone CEM (Figure

Received: August 17, 2023
Accepted: October 11, 2023
Published: October 16, 2023

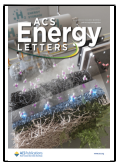

https://doi.org/10.1021/acsenergylett.3c01716
ACS Energy Lett. 2023, 8, 4674−4683

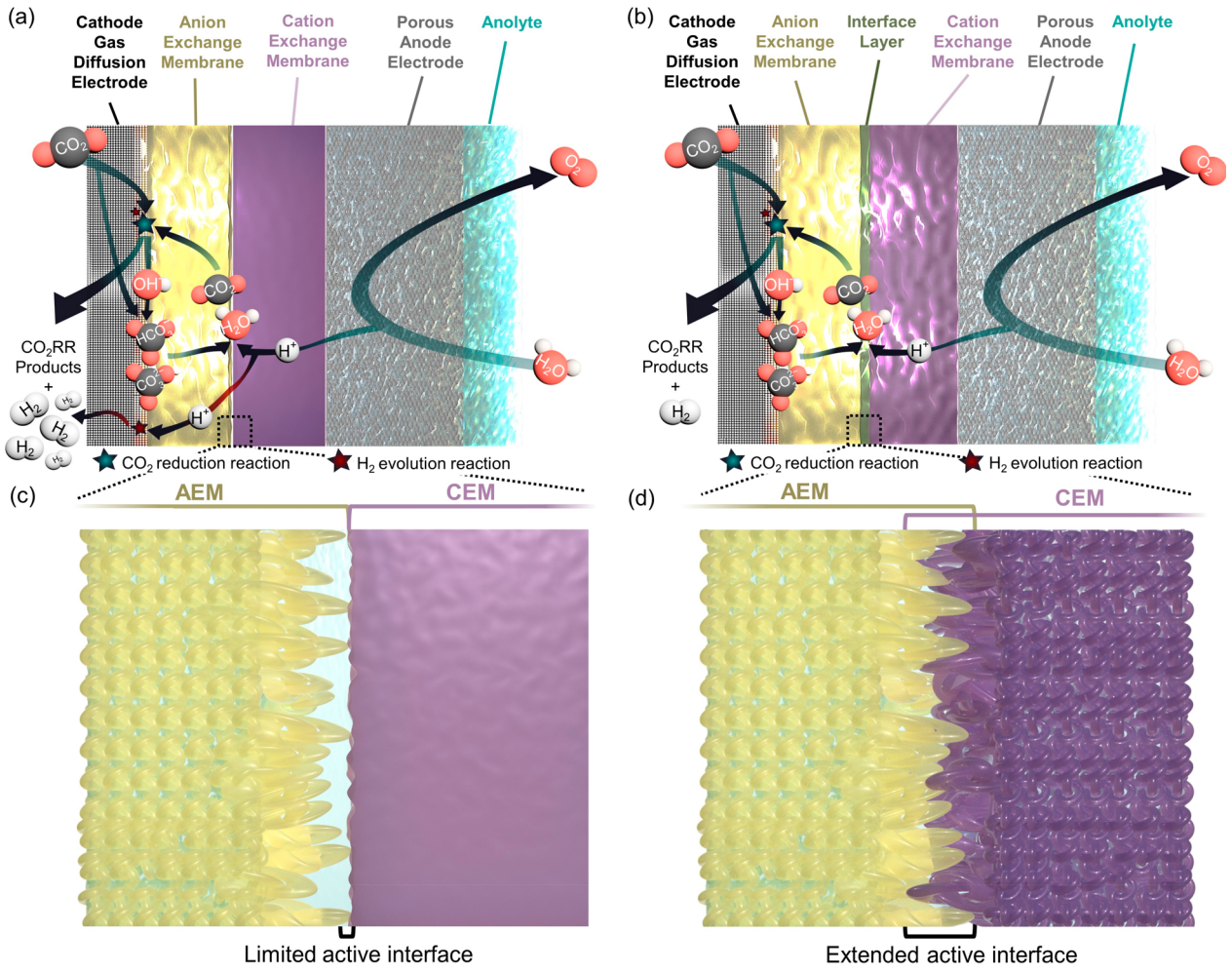

Figure 1. Theoretical understanding of bipolar membrane (BPM) systems with different interfaces operating in the forward-bias mode. (a) A control system schematic in which the anion exchange membrane (AEM) is sprayed onto the cathode, and a commercial cation exchange membrane (CEM) is used. This system suffers from H_2 evolution. (b) A direct membrane deposition (DMD) system schematic in which the AEM is sprayed onto the cathode and the CEM is sprayed onto the AEM. Not to scale (each drawn layer width is increased/decreased for clarity). Enlarged view of the contact between AEM and CEM, resulting in different levels of AEM|CEM interface "activity" in (c) the control system and in (d) the DMD system.

1a,c)—the standard approach in CO_2RR f-BPM electrolyzers.[7] Although commercial BPMs have well-connected AEM and CEM layers and can be operated in forward-bias mode,[11,12] they are prone to blistering.[7,8,11,13] Alternatively, when a membrane layer is sprayed, the outermost membrane surface is rougher than that of commercially produced membranes (Figure S1).[14,15] In the presence of electrolyte, membranes can also experience swelling,[16] leading to additional stress at the membrane−membrane interface. Therefore, gaps between the AEM and CEM are expected when an AEM is sprayed upon a cathode and then assembled with a commercial CEM. The result is a low AEM|CEM interfacial area (Figure 1c) with greater potential for mechanical and electrochemical performance loss via blistering and reduced ion exchange. In addition, achieving CO_2 regeneration and preventing proton crossover to the cathode require the proton flux from the anode to be balanced with (bi)carbonate flux from the cathode at the AEM|CEM interface. We reasoned that controlling the AEM|CEM interface is crucial for achieving efficient CO_2 regeneration in an f-BPM and that a well-connected interface would result if the CEM material infiltrated the AEM, creating a conformal interface and a monolithic composite membrane (Figure 1b,d).

In this work, we develop a direct membrane deposition (DMD) approach to fabricate a monolithic AEM|CEM membrane composite structure within a CO_2RR MEA electrolyzer. The DMD approach creates a seamless and continuous interface between the AEM and CEM, provides access to ion and gas transport domains, and can thereby exceed the performance achieved with commercial membranes of fixed structure and thickness. We find that a conformal AEM|CEM interface increases ion mass transport by up to 58%, enabling efficient CO_2 regeneration without blistering. By customizing the AEM and CEM membrane thicknesses, we obtain a C_{2+} FE of 65% and a H_2 FE of 12% at 300 mA cm^{-2}. We also demonstrate an SPC of 69% at 300 mA cm^{-2} with 42% C_{2+} selectivity, enabling an over 2-fold increase in partial current density performance over best prior existing carbon-efficient f-BPM CO_2RR MEA electrolyzers at the highest reported SPC.

We first prepared the cathode by sputtering 200 nm of a copper catalyst on a porous polytetrafluoroethylene gas diffusion layer. We started by employing a commercial standalone AEM in the electrolyzer. The AEM facilitated HCO_3^- and CO_3^{2-} anion migration to the anode, where these

https://doi.org/10.1021/acsenergylett.3c01716
ACS Energy Lett. 2023, 8, 4674−4683

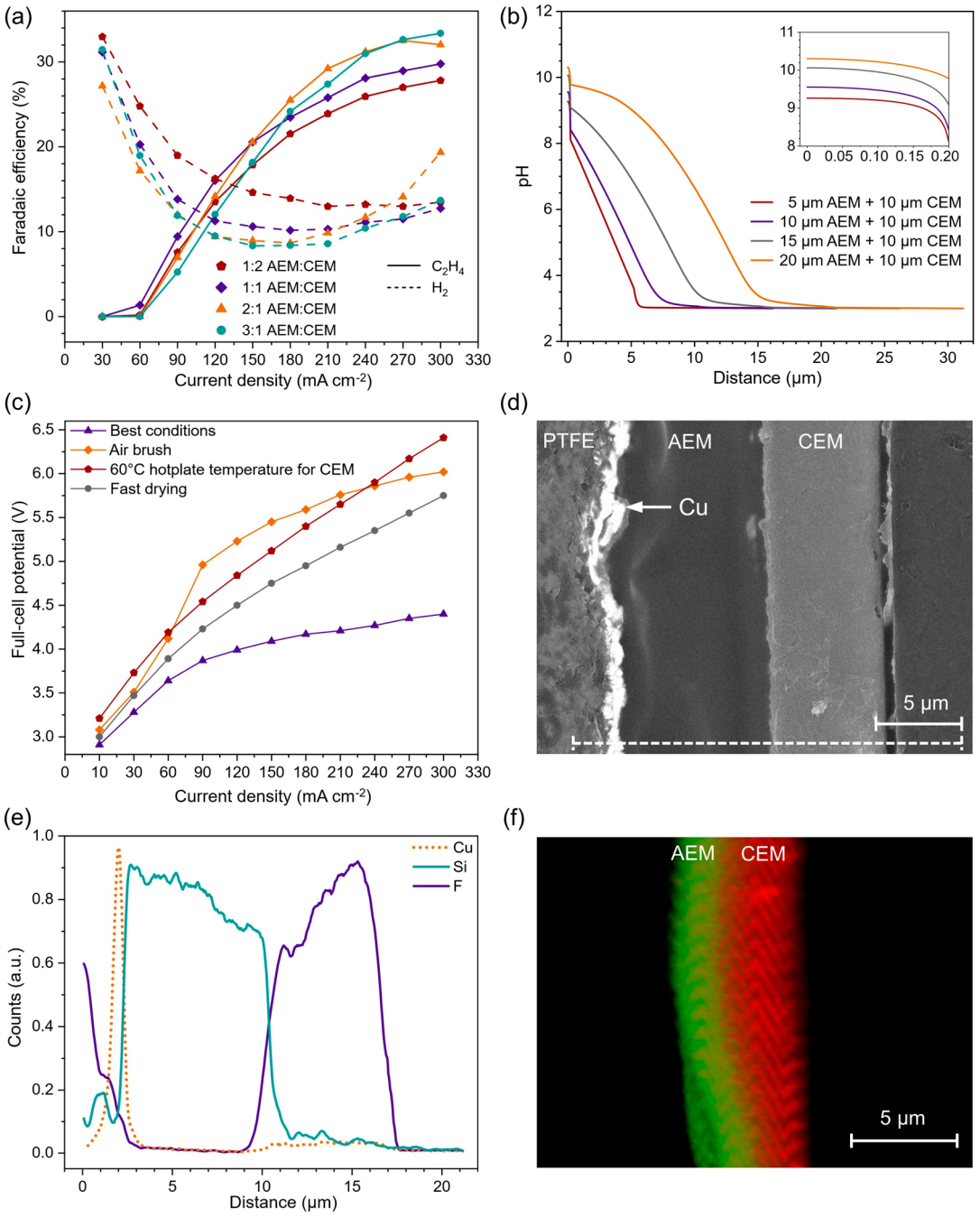

Figure 2. Direct membrane deposition (DMD) performance and characterization. (a) Ethylene and H_2 FEs of asymmetric 2 mg cm^{-2} BPMs in DMD systems. (b) pH simulation at increasing AEM thickness, 1 μm interface layer (IL), and 10 μm CEM. The inset represents an enlarged view of the catalyst layer. The simulation assumed operation at 100 mA cm^{-2} with an 85% CO_2RR FE and 15% H_2 FE. (c) Performance of a 1:1 AEM:CEM (2 mg cm^{-2} BPM) DMD system under different deposition conditions. Details are given in Figure S11. (d) Scanning electron microscopy (SEM) image of a 1:1 AEM:CEM (2 mg cm^{-2} BPM) DMD sample. (e) Energy dispersive X-ray (EDX) line scan obtained over a cross-section of the sample (shown as a dashed line in the SEM image). All samples were prepared using automatic spray coating unless otherwise specified. (f) Confocal microscopy image of a 1:1 AEM:CEM (1 mg cm^{-2} BPM) DMD sample prepared using manual air brushing. Half the typical 2 mg cm^{-2} BPM loading was used to prepare this sample to allow for light penetration during confocal microscopy.

anions oxidize and form CO_2.[17] The result is high CO_2 crossover (up to 70%),[7] evidenced by the low percentage of CO_2 detected at the cathode outlet (~6% CO_2) despite high HER (i.e., low CO_2 conversion is expected with 61% H_2 FE at 300 mA cm^{-2}; Figure S2). When a standalone commercial CEM is employed as the sole membrane, high H_2 evolution is obtained (Figure S2), a result attributed to the high concentration of protons at the cathode surface.[18] A thicker CEM can result in nearly 100% H_2 FE.[7] To mitigate the issues of CO_2 crossover and high proton concentration, we investigated an f-BPM for its potential to decrease H_2 production (by creating alkaline conditions at the cathode surface) and maintain low CO_2 crossover to the anode (via the combination of HCO_3^- and CO_3^{2-} ions with protons at the

https://doi.org/10.1021/acsenergylett.3c01716
ACS Energy Lett. 2023, 8, 4674−4683

AEM|CEM interface). The f-BPM was constructed via the DMD approach by spray coating, onto the cathode, the AEM and then the CEM (see the Supporting Information and Figure S3 for more details). The non-DMD control case f-BPM comprised an AEM sprayed on the copper cathode with a commercial CEM placed on top.[7] Automated spray coating was used for both the DMD and control case BPMs, unless otherwise noted. In all cases, a commercial IrO_2 on Ti felt anode completed the assembly, and deionized water (unless otherwise specified) was employed as the anolyte.

The fully deposited BPM system was compared to an otherwise similar control system (which uses a commercial CEM) to study the effect of interface conformity on the performance of the CO_2 electrolyzer. We first prepared BPMs with membrane thicknesses similar to those in the control system. The control system comprised of 1 mg cm^{-2} of AEM and a commercially available nonreinforced CEM (N211, 25 μm).[19] While a reinforced membrane could provide greater mechanical strength, a lack of adhesion between ionic and reinforcing materials can result in mechanical breakdown and reduced ionic selectivity.[20] In addition, the relative amount of ion exchange material and reinforcing agent is not readily apparent in commercial reinforced membranes. Therefore, all membranes used in this work were fabricated without reinforcing materials. Scanning electron microscopy (SEM) showed roughly 6−8 μm for 1 mg cm^{-2} of membrane (Figure S1). The DMD system was fabricated with 1 mg cm^{-2} of AEM and 4 mg cm^{-2} of CEM (1:4 AEM:CEM; i.e., 30−40 μm total BPM thickness). Electrochemical testing showed less H_2 FE in the DMD system compared to that in the control system across the range of applied current densities (Figure S4). Since the major difference between these two systems is the sprayed vs separate nature of the CEM, the performance improvement is attributed to the conformity of the sprayed CEM on the rough AEM surface, leading to the improved pathways for protons and (bi)carbonate ions (Figure 1c,d).

The DMD approach further enables customization of the ratio of AEM to CEM within the BPM.[21] Commercial CEMs are limited to set $\geq$5 μm thicknesses that enable them to be handled individually.[22] Here, DMD was employed to access thin CEMs. Using a DMD system with 1 mg cm^{-2} of AEM and 1 mg cm^{-2} of CEM (1:1 AEM:CEM with 2 mg cm^{-2} BPM), we found a thinner CEM led to a reduction in H_2, CO, and formate FEs and an increase in C_{2+} FE, compared to the 1:4 AEM:CEM (5 mg cm^{-2} BPM) DMD system (Figure S5). Similar trends were observed by varying the AEM:CEM ratio in a 2 mg cm^{-2} BPM DMD system (Figure 2a and Figure S6). COMSOL simulation was employed to screen different AEM:CEM ratios and analyze the CO_2RR operation (see the Supporting Information, Figure S7, and Tables S1 and S2 for details). A higher AEM:CEM ratio led to higher pH and CO_2 availability in the cathode catalyst layer (Figure 2b and Figure S8)—a result we ascribe to a balance achieved via reduced proton crossover (Figure S9) and increased (bi)carbonate ion transport.[12,13,23,24] Therefore, a higher AEM:CEM ratio leads to a lower H_2 FE and higher C_{2+} product formation (enabled by the higher alkalinity) (Figure 2a). However, a threshold in performance was observed, where a high AEM:CEM ratio (4:1) led to the formation of H_2 at the expense of CO_2RR products (Figure S6). At this extreme ratio, the membrane transitions to being almost entirely composed of AEM. We tested the CO_2RR in an AEM-only DMD system with a neutral pH electrolyte (0.1 M $KHCO_3$). The observed gas FEs for this setup (Figure S10) were similar to those obtained in the 4:1 AEM:CEM ratio DMD system (Figure S6). The full-cell potential for the AEM-only DMD system was also higher than that of the control system employing a standalone AEM. Although the infiltration of AEM into the catalyst layer pores in the DMD system could be expected to enhance ionic conductivity in the catalyst layer and decrease interfacial losses, it seems that it hindered the CO_2 gas to liquid phase transport in the coated portion of the catalyst layer.[15,25] Therefore, decreased ethylene production and increased HER values are observed at high current densities in this system.

We noticed that the BPM preparation conditions were crucial to the DMD system performance (Figure 2c and Figure S11). Using manual air brushing to spray the membranes resulted in high HER with increasing current density (>26% at >240 mA cm^{-2}), while using an automatic spray coater resulted in lower H_2 FE, in the range of ∼10−12%. The ethylene peak also changed from 150 to 300 mA cm^{-2} for manual air brushing vs automatic spray coating, respectively. Through measuring the thickness distribution over a ∼2 mm length of the automatic spray coated membrane (Figure S12), the total BPM thickness was found to be 17.1 ± 0.2 μm (s.e.m.). In electrochemical testing, we found this thickness to be optimal in terms of the product FE and full-cell potential. Thicker BPMs elongate the distance between the AEM|CEM interface and the cathode, which limits the transport of regenerated CO_2 to the cathode and entails a higher full-cell potential due to the increased membrane resistance (Figure S13). The longer diffusion distance for dissolved CO_2 in thicker membranes causes an exacerbated HER, especially with increasing current density. Thinner BPMs (e.g., total thickness of <12 μm) were found to cause short-circuiting. The manually air brushed membrane showed ∼6.6 μm in total thickness (Figure S14). The difference in membrane thickness obtained through automatic spray coating and manual air brushing indicates that the deposition method can affect the final membrane density and free volume.[26] A less dense membrane has more connected hydrophilic domains that enable higher ion diffusion and conductivity (Figure S14),[26] which could explain the lower full-cell potential observed for the automatic spray coated membrane (Figure 2c). Fourier transform infrared (FTIR) spectroscopy showed no change in CEM structure between automatically spray coated and manually air brushed membranes (Figure S15).

The conditions of the automatic spray coating were also observed to affect performance. During automatic spray coating at room temperature, the AEM dried instantly, even as more layers were sprayed. However, the CEM took longer to dry, forming a wet surface over the AEM as more layers were sprayed. To examine the effect of membrane conformity, we increased the rate of solvent evaporation during CEM spraying. Faster drying of the CEM resulted in an elevated full-cell potential during electrochemical testing (Figure 2c) and shifted the gas FE distribution toward a higher proportion of CO (Figure S11). These experiments implied that the AEM|CEM interface is better interlinked when the samples are sprayed and dried slowly at room temperature, ensuring that the wet CEM infiltrates the voids at the top of the AEM surface. The morphology and porosity of the sprayed membranes have been previously reported to be impacted by solvent selection and drying temperature.[26−28] We hypothesized that the microscale integration of the polymers in the interface layer (through phase segregation, interface thickness,

https://doi.org/10.1021/acsenergylett.3c01716
ACS Energy Lett. 2023, 8, 4674−4683

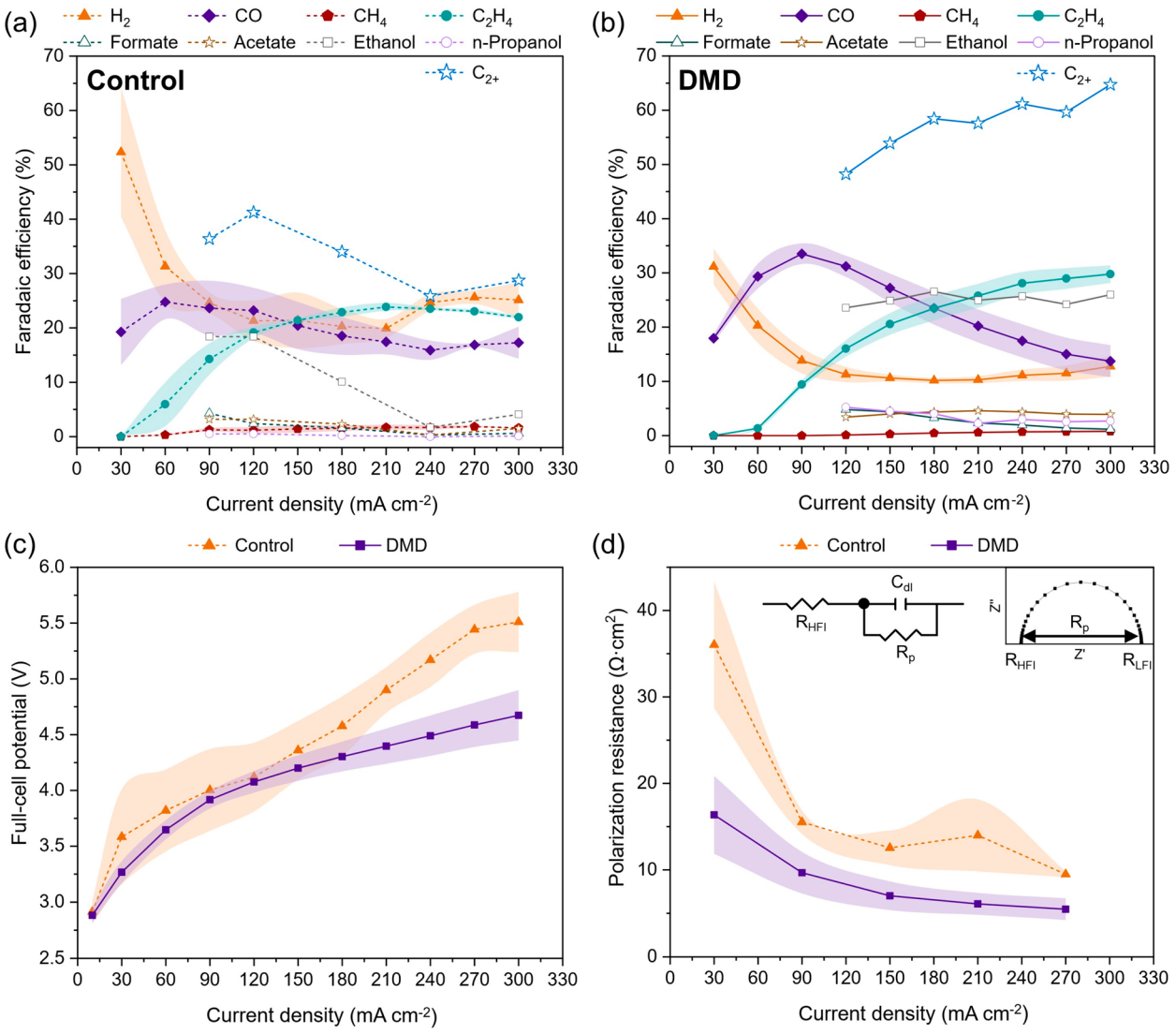

Figure 3. Performance comparison between the control and the 1:1 AEM:CEM (2 mg cm^{-2} BPM) DMD system at varying current densities. Faradaic efficiency obtained from (a) the control and (b) the DMD system. (c) Comparison of the obtained full-cell potential between the control and DMD systems. (d) Comparison of the polarization resistance (R_p) between the control and DMD systems obtained through electrochemical impedance spectroscopy (EIS) at varying current densities. The inset shows an example of a Nyquist plot in which R_p is calculated by subtracting the high-frequency intercept (R_{HFI}) from the low-frequency intercept (R_{LFI}). The equivalent circuit model used in fitting the experimental EIS data is also shown. The data are the mean of three experiments using identical samples. The connected error bars represent the standard error. All samples were prepared using automatic spray coating.

and morphology) also impacts ion and mass transport and overall BPM performance.[12]

We employed SEM to assess the AEM|CEM interface. The CEM was observed to fill the corrugated surface of the AEM, resulting in a conformal geometry between the two membranes (Figure 2d). We used energy dispersive X-ray (EDX) spectroscopy to investigate the elemental composition of the membranes (Figure 2e). EDX showed regions of Si and F signals in the BPM, corresponding to the AEM and CEM materials, respectively. Wet silicon carbide paper, which forms silanol groups in water, was used to polish the samples before imaging. Upon dissociation, silanol groups form SiO^-.[29] The observed Si signal can thus be attributed to negatively charged SiO^- ions that adhered to the positively charged backbone of the AEM during sample polishing. The EDX line scan shows continuous Si and F signals, suggesting the possibility of interlinked AEM and CEM polymer chains. However, due to the resolution limitations of the EDX scan, it was only possible to confirm that the AEM|CEM interface is conformal. To investigate further, confocal microscopy was employed, and the AEM and CEM were stained with colored dyes. This approach evidenced the interlinking of AEM and CEM structures (Figure 2f, Figure S16, and SI Video 1).

To evaluate the benefit of a conformal AEM|CEM interface, we compared the performance of the 1:1 AEM:CEM (2 mg cm^{-2} BPM) DMD system to that of the control system over a range of current densities. The DMD system demonstrated consistently low H_2 FE (Figure 3a,b). At high current density (300 mA cm^{-2}), the DMD system achieved a peak FE of 33% C_2H_4, 26% ethanol, and 12% H_2, compared to 22%, 4%, and 25%, respectively, in the control system. The lower H_2 FE in the DMD system indicates that fewer protons were able to reach the catalyst surface and participate in the HER than in the control case, while the improved C_{2+} FE could indicate

https://doi.org/10.1021/acsenergylett.3c01716
ACS Energy Lett. 2023, 8, 4674−4683

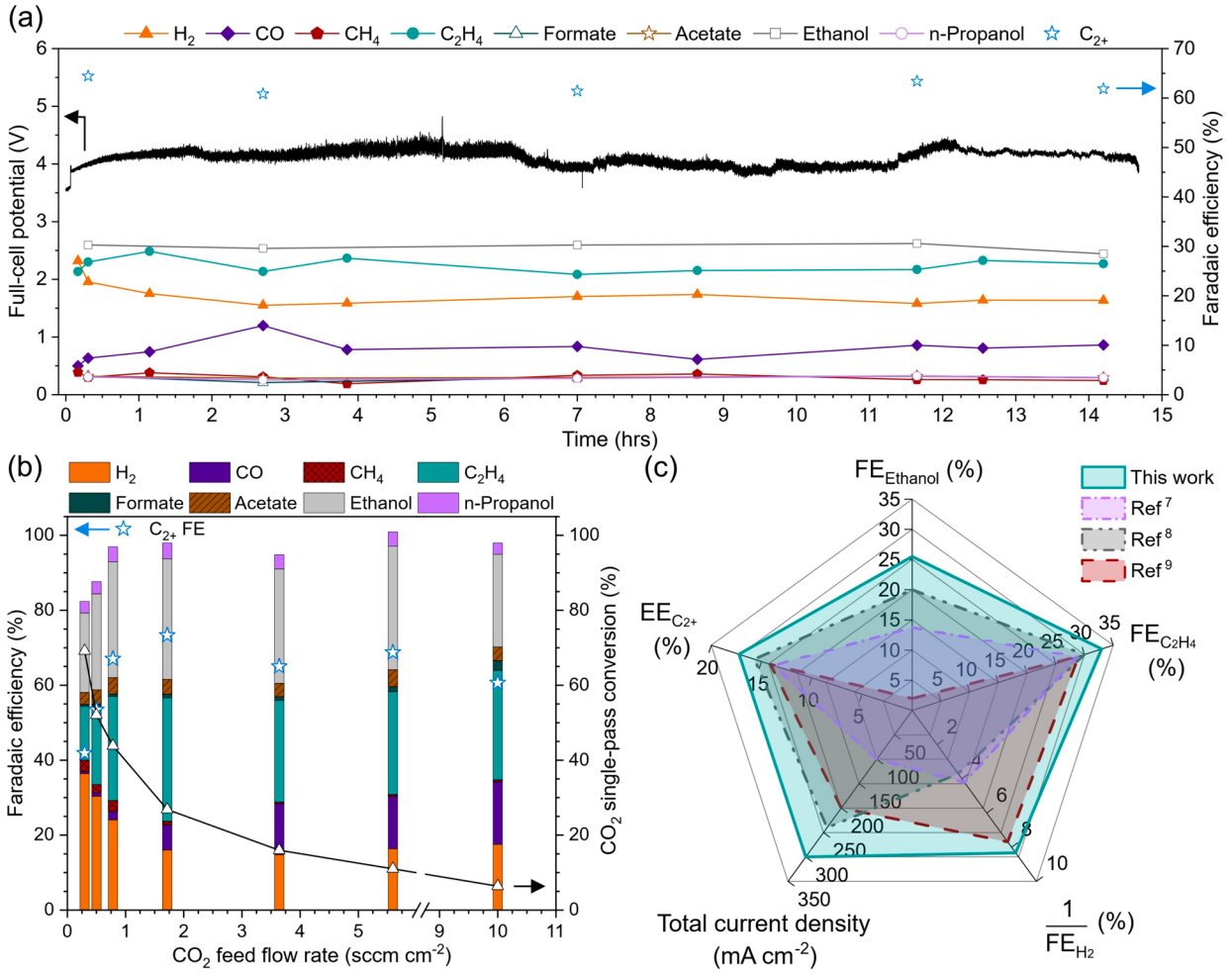

Figure 4. DMD system assessment and comparison to state-of-the-art forward-bias BPM CO_2 electrolyzers. (a) Stability of full-cell potential and products over time while operating at 150 mA cm^{-2} in a 1:1 AEM:CEM (2 mg cm^{-2} BPM) DMD system. (b) CO_2 single-pass conversion and product FEs as the CO_2 inlet flow rate was changed while operating at 300 mA cm^{-2} in a 1:1 AEM:CEM (2 mg cm^{-2} BPM) DMD system. The samples were prepared using automatic spray coating. (c) Performance comparison of this work against the current CO_2 f-BPM literature. The presented literature data are based on the highest operating current density with reported liquid products (Table S4).

higher CO_2 availability and higher local pH conditions. We also investigated the performance of another control setup (herein called Control 2) in which the AEM is directly sprayed onto a commercial CEM (N211). Control 2 showed high H_2 FE and poor ethylene FE (<8%) over current density (Figure S17). Blistering was also observed after electrochemical testing. The nonsprayed nature of the CEM in Control 2 likely has lower free volume between the polymer chains than a sprayed CEM, which can lead to the entrapment of regenerated CO_2 and H_2O at the AEM|CEM interface. Therefore, the fully sprayed membranes in the DMD system are expected to facilitate ion and water transport and enable enhanced performance compared with the membrane configurations used in the tested controls.

Over the range of applied current densities, the DMD system exhibited lower operating full-cell potential than in the control system (e.g., 4.67 and 5.51 V, respectively, or 0.84 V less than the control system, at 300 mA cm^{-2}; Figure 3c). In both systems, the anolyte pH at the end of electrolysis was similar (Figure S18), indicating a negligible contribution of the Nernst pH overpotential to the observed differences in full-cell potential. To better understand the root cause of the lower full-cell potential in the DMD case, electrochemical impedance spectroscopy (EIS) was applied during operation. The high-frequency intercept resistance, or R_{HFI}, associated with electronic resistance, membrane Ohmic resistance, and contact resistance,[30] was found to be similar for the DMD and control systems (Figure S19). Thus, the reduced full-cell potential observed in the DMD system cannot be attributed to the reduced total BPM thickness.[31] Charge transfer resistance, catalyst layer ionic resistance, and mass transport resistance were interpreted from the polarization resistance, or R_p.[32] At each applied current density, the DMD system showed a lower R_p than the control system (Figure 3d and Figure S20), even at high current densities (e.g., at 270 mA cm^{-2}, the DMD showed an R_p of ~5.5 Ω cm^2, while the control system showed ~9.5 Ω cm^2). The charge transfer resistance and the catalyst layer ionic resistance were assumed to be similar between the DMD system and the control system due to the use of the same cathode and AEM material and thicknesses in both cases. Thus, the mass transport resistance can be associated with the observed R_p at each current density. Since the DMD system ensures better connectivity via well-linked AEM and CEM ionomers, it provides improved mass transport (including ions, water, and dissolved gases) along with more effective ion neutralization at the interface, leading to lower R_p (Figure 3d).

https://doi.org/10.1021/acsenergylett.3c01716
ACS Energy Lett. 2023, 8, 4674−4683

The observed full-cell potentials are expected to be affected by the kinetics of the recombination of HCO_3^-, CO_3^{2-}, and OH^- with H^+ at the AEM|CEM interface. Grew et al. described a trap-assisted mechanism for water recombination in f-BPMs, where fixed ionic charged groups of both membranes facilitate water recombination.[33,34] Developing corrugated membrane surfaces can increase the interfacial contact between the AEM and CEM (as was demonstrated through the DMD approach), thereby decreasing the possible voltage losses associated with ion recombination.[33] The development of BPMs with improved interface activity is also expected to decrease water transport limitations and result in lower full-cell potentials.[13] Prior reports additionally suggested that water recombination in forward-bias mode is not affected by the electric field.[12,35,36] However, in the case of CO_2RR, the presence of (bi)carbonate ions in the AEM reduces the pH in the AEM and reduces the AEM conductivity compared to only having OH^- ions in a water electrolyzer. This operation decreases the voltage difference across the AEM|CEM interface (i.e., junction potential) and, hence, reduces the electric field, which affects the full-cell potential by an estimated minimum of 0.2 V.[33] With proton transport being 2−8 times faster than OH^- transport (and even higher compared to (bi)carbonate ion transport),[37] the transport of anions (i.e., HCO_3^-, CO_3^{2-}, and OH^-) in the AEM of the CO_2RR f-BPM is expected to be the rate-determining step in recombination kinetics.

With extended run times, the DMD system maintained continuous operation for over 14 h at 150 mA cm^{-2}, achieving an average of 4.11 V, 26% C_2H_4 FE, 30% ethanol FE, 20% H_2 FE, and 62% C_{2+} FE (Figure 4a). SEM imaging of the DMD system confirmed the integrity of the BPM postelectrolysis (Figure S21). In the DMD system, no blistering, bubbles, or delamination in the membrane was observed directly after testing (Figure S22). The porous membrane structure obtained through the DMD approach possibly enhanced water permeability through offering more connected hydrophilic domains.[26] Greater water permeability and removal can decrease hydraulic and Maxwell pressures acting to drive water into the BPM interface, which decreases the chance of blistering and delamination.[38] The composite AEM|CEM structure also reduces water buildup in the f-BPM.[12] FTIR spectroscopy was applied on DMD samples before and after electrolysis to study the chemical structure evolution in the membrane. No changes were detected in the CEM structure (Figure S23),[2] suggesting the stable structure of the membrane. During electrochemical testing, the DMD system demonstrated a stable full-cell potential, while the control system showed an increasing full-cell potential trend at each applied current density (Figure S24). This voltage creep implies incomplete ion neutralization and CO_2 transport in the control system due to a lack of full contact between the AEM and CEM. This instability could also indicate gas entrapment between the AEM and CEM in the control system.[39]

We investigated the effect of cell temperature on the CO_2 electrolysis performance. Applying higher cell temperatures (40 and 60 °C) reduced the operating full-cell potential (Figure S25), which is enabled by the higher ionic conductivity achieved with higher temperatures. However, higher H_2 evolution was observed at the higher cell temperatures, which could be caused by the reduced CO_2 solubility and the promotion of HER kinetics. Therefore, applying a higher cell temperature might be a lever for decreasing the full-cell potential, yet further improvements are needed to suppress H_2 evolution.

Employing a different anolyte pH can also affect the electrolysis performance. When we conducted a test with 1 M KOH as the anolyte in the 1:1 AEM:CEM (2 mg cm^{-2} BPM) DMD system, we observed low ethylene selectivity and a tendency toward H_2 (Figure S26). In this MEA configuration, salt formation is expected at the AEM|CEM interface or at the catalyst surface.[40] Nevertheless, upon completion of the test and examination of the cathode and flow field, there were no indications of salt formation. However, the cathode surface appeared wet, suggesting that water might have been electro-osmotically dragged to the cathode via the K^+ ions, which could also account for the high H_2 FE. The water migration could also contribute to eliminating any salt formation that might have occurred during electrolysis. After leaving the tested MEA on the bench for 1 h, the cathode showed signs of degradation and BPM delamination. On the other hand, conducting tests with 0.01 M H_2SO_4 as the anolyte yielded comparable gas FE results to DI water, albeit with slightly lower ethylene (28% ethylene and 13% H_2 at 300 mA cm^{-2}; Figure S26). These FEs suggest that the DMD system can shield the cathode from high proton concentration while maintaining satisfactory performance. The acidic anolyte also reduced the full-cell potential compared to DI water, which can be attributed to the superior ionic conductivity of the former.[13]

The greater free volume between membrane polymer chains in the DMD case combined with a lower membrane thickness could be expected to increase the product crossover. However, the gas collected from the anolyte chamber showed low amounts of cathode-produced gases (Figure S27), with a maximum of ∼1% C_2H_4 FE and ∼4% H_2 FE in the thinnest DMD system tested (1:1 AEM:CEM with 2 mg cm^{-2} BPM and ∼17 μm total thickness). The control system showed <1% of each gas. The DMD system also exhibited a maximum SPC of 69% at 0.3 sccm cm^{-2} of inlet CO_2 flow rate with 42% C_{2+} FE (Figure 4b). A maximum C_{2+} FE of 73% was achieved at 1.7 sccm cm^{-2} and 27% SPC (Figure 4b). This SPC performance surpasses previous CO_2 f-BPM demonstrations[7−9] while operating at a high current density (300 mA cm^{-2}) (Table S3). The presented system configuration improved product selectivity and decreased H_2 evolution when operating at a high current density compared to the state-of-the-art CO_2 f-BPM electrolyzers (Figure 4c and Tables S4 and S5). The DMD system also increased the full-cell energy efficiency (EE) compared to previous reports (Figure 4c) and the control system (Figure S28 and Table S6), achieving a 17.2% EE for C_{2+} products at 300 mA cm^{-2} and 10 sccm cm^{-2}.

To test the general applicability of the DMD approach, we evaluated the performance of a DMD BPM system and a control system equipped with a CO-producing silver-based cathode. At 90 mA cm^{-2}, the DMD system achieved a maximum of 90% CO FE and 2% H_2 FE compared to 65% and 6%, respectively, in the control system (Figure S29). The control system failed to operate beyond 90 mA cm^{-2}, whereas the DMD system reached 240 mA cm^{-2}. In this operating current density range, EIS showed a higher polarization resistance in the control system compared to that in the DMD system (Figure S29). The R_{HFI} values for both systems were similar (Figure S29). These results indicate the effectiveness of the DMD approach in reducing mass transport resistance in both copper- and silver-based CO_2 f-BPM MEA electrolyzers.

https://doi.org/10.1021/acsenergylett.3c01716
ACS Energy Lett. 2023, 8, 4674−4683

In this work, DMD was employed to develop integrated MEAs with BPMs in forward-bias mode for CO_2 electrolysis. We found that a controlled reduction in the ratio of CEM thickness with respect to the AEM thickness decreased the proton crossover from the anode to cathode and, thereby, resulted in less H_2 generation. The extended active AEM|CEM interface offered by the DMD approach reduced the ion mass transport resistance, achieving a 0.84 V improvement in the full-cell potential at 300 mA cm^{-2}. Further reduction in the full-cell potential can be achieved by employing higher conductivity anolytes or by increasing the cell temperature, although further optimization will be needed to suppress H_2 evolution in such cases. Employing DMD enabled the control of membrane conformity, thickness, and composition, which enhanced the CO_2 regeneration and system performance. The DMD approach demonstrated here presents further opportunities for optimization, including the continuous blending of membrane chemistries and properties, the incorporation of additional layers, and the deep integration of catalysts—all within a serial spray application process that is amenable to scaled manufacturing.

■ ASSOCIATED CONTENT

Supporting Information

The Supporting Information is available free of charge at https://pubs.acs.org/doi/10.1021/acsenergylett.3c01716.

Confocal microscopy video (MP4)

Experimental materials and methods, COMSOL modeling description, SEM and atomic force microscopy of AEM DMD on sputtered Cu, AEM and CEM control tests, spray coater paths sketch, performance comparison using similar membrane thicknesses, DMD performance at different AEM:CEM ratios, modeling details schematic, simulated CO_2 and proton concentration at different AEM:CEM ratios, performance in an AEM DMD system, effect of deposition conditions on electrolyzer performance, DMD thickness measurement distribution, DMD performance at different BPM thicknesses, SEM, EIS, and FTIR of automatically and manually prepared samples, confocal microscopy line scan, Control 2 performance, anolyte pH over time, comparison of R_{HFI}, Nyquist plots at different current densities, SEM and real images of the electrolyzer before and after operation, FTIR spectra before and after electrolysis, time-dependent full-cell potential comparison, performance at different cell temperatures or anolyte pH, gas product crossover, energy efficiency comparison, performance with a silver-based cathode, modeling details tables, and performance summary tables (PDF)

■ AUTHOR INFORMATION

Corresponding Authors

Nana Zhao − *Energy, Mining & Environment Research Centre, National Research Council Canada, Vancouver, British Columbia V6T 1W5, Canada*; Email: Nana.Zhao@nrc-cnrc.gc.ca

David Sinton − *Department of Mechanical and Industrial Engineering, University of Toronto, Toronto, Ontario M5S 3G8, Canada*; orcid.org/0000-0003-2714-6408; Email: sinton@mie.utoronto.ca

Authors

Tartela Alkayyali − *Department of Mechanical and Industrial Engineering, University of Toronto, Toronto, Ontario M5S 3G8, Canada*; orcid.org/0000-0003-3895-8700

Ali S. Zeraati − *Department of Mechanical and Industrial Engineering, University of Toronto, Toronto, Ontario M5S 3G8, Canada*

Harrison Mar − *Department of Forest Resources Management, University of British Columbia, Vancouver, British Columbia V6T 1Z4, Canada*

Fatemeh Arabyarmohammadi − *Department of Mechanical and Industrial Engineering, University of Toronto, Toronto, Ontario M5S 3G8, Canada*

Sepehr Saber − *Department of Mechanical and Industrial Engineering, University of Toronto, Toronto, Ontario M5S 3G8, Canada*

Rui K. Miao − *Department of Mechanical and Industrial Engineering, University of Toronto, Toronto, Ontario M5S 3G8, Canada*

Colin P. O'Brien − *Department of Mechanical and Industrial Engineering, University of Toronto, Toronto, Ontario M5S 3G8, Canada*

Hanshuo Liu − *Energy, Mining & Environment Research Centre, National Research Council Canada, Vancouver, British Columbia V6T 1W5, Canada*

Zhong Xie − *Energy, Mining & Environment Research Centre, National Research Council Canada, Vancouver, British Columbia V6T 1W5, Canada*

Guangyu Wang − *Department of Forest Resources Management, University of British Columbia, Vancouver, British Columbia V6T 1Z4, Canada*

Edward H. Sargent − *Department of Electrical and Computer Engineering, University of Toronto, Toronto, Ontario M5S 1A4, Canada*; orcid.org/0000-0003-0396-6495

Complete contact information is available at: https://pubs.acs.org/10.1021/acsenergylett.3c01716

Author Contributions

⊥T.A., A.S.Z., and H.M. contributed equally to this work.

Author Contributions

Z.X., G.W., E.H.S., N.Z., and D.S. supervised the project. T.A. conceived the idea, designed and carried out the electrochemical experiments, performed the COMSOL simulation, and performed SEM, EDX, and EIS analyses. A.S.Z. and F.A. helped with liquid product analysis, electrochemical testing, and SPC evaluation. A.S.Z. performed FTIR analysis. H.M. performed many electrochemical experiments and EIS analyses. S.S. performed confocal microscopy imaging. R.K.M. prepared sputtered Cu and Nafion samples. R.K.M. and C.P.O. provided experimental advice. H.L. helped with SEM and EDX. All authors contributed to the discussion and editing of the manuscript.

Notes

The authors declare no competing financial interest.

■ ACKNOWLEDGMENTS

Experiments were conducted in the laboratories of the Energy, Mining and Environment Research Centre at the Vancouver National Research Council Canada (NRC), British Columbia and at the University of Toronto. The authors acknowledge Peter Mardle, Ken Tsay, Ken Shi, Zhengming Jiang, Wei Qu, Jason Fahlman, Elizabeth Fisher, Shaochen Ding, Weimin

Qian, and Nadia Zavala of the NRC for their technical help and discussions regarding the experiments. Ruoxi Qiao is acknowledged for conducting preliminary SEM and EDX imaging. Jonathan P. Edwards, Walid Mazyan, and Prasad Sarma are thanked for useful discussions. The Centre for Research and Applications in Fluidic Technologies (CRAFT) is acknowledged for the use of their confocal microscope under the Canada Foundation for Innovation/Ontario Research Fund grant 36442. The authors acknowledge the NRC and the University of Toronto Collaboration Centre Program in Green Energy Materials (CC-GEM, GEM-PRJ-01) for providing funding for this project. This work also received financial support from the Natural Sciences and Engineering Research Council of Canada (NSERC). D.S. acknowledges the support received from the Canada Research Chairs program. T.A. thanks Hatch, NSERC, and the University of Toronto for their support through graduate scholarships and fellowships.

REFERENCES

(1) Gabardo, C. M.; O'Brien, C. P.; Edwards, J. P.; McCallum, C.; Xu, Y.; Dinh, C. T.; Li, J.; Sargent, E. H.; Sinton, D. Continuous Carbon Dioxide Electroreduction to Concentrated Multi-Carbon Products Using a Membrane Electrode Assembly. *Joule* **2019**, *3* (11), 2777−2791.

(2) Adnan, M. A.; Zeraati, A. S.; Nabil, S. K.; Al-Attas, T. A.; Kannimuthu, K.; Dinh, C.-T.; Gates, I. D.; Kibria, M. G. Directly-Deposited Ultrathin Solid Polymer Electrolyte for Enhanced CO_2 Electrolysis. *Adv. Energy Mater.* **2023**, *13*, No. 2203158.

(3) Burdyny, T.; Smith, W. A. CO_2 Reduction on Gas-Diffusion Electrodes and Why Catalytic Performance Must Be Assessed at Commercially-Relevant Conditions. *Energy Environ. Sci.* **2019**, *12* (5), 1442−1453.

(4) Kibria, M. G.; Edwards, J. P.; Gabardo, C. M.; Dinh, C. T.; Seifitokaldani, A.; Sinton, D.; Sargent, E. H. Electrochemical CO_2 Reduction into Chemical Feedstocks: From Mechanistic Electrocatalysis Models to System Design. *Adv. Mater.* **2019**, *31* (31), 1−24.

(5) Rabinowitz, J. A.; Kanan, M. W. The Future of Low-Temperature Carbon Dioxide Electrolysis Depends on Solving One Basic Problem. *Nat. Commun.* **2020**, *11* (1), 10−12.

(6) Ozden, A.; Garcia de Arquer, F. P.; Huang, J. E.; Wicks, J.; Sisler, J.; Miao, R. K.; O'Brien, C. P.; Lee, G.; Wang, X.; Ip, A. H.; Sargent, E. H.; Sinton, D. Carbon-Efficient Carbon Dioxide Electrolysers. *Nat. Sustain.* **2022**, *5*, 563−573.

(7) O'Brien, C. P.; Miao, R. K.; Liu, S.; Xu, Y.; Lee, G.; Robb, A.; Huang, J. E.; Xie, K.; Bertens, K.; Gabardo, C. M.; Edwards, J. P.; Dinh, C.-T.; Sargent, E. H.; Sinton, D. Single Pass CO_2 Conversion Exceeding 85% in the Electrosynthesis of Multicarbon Products via Local CO_2 Regeneration. *ACS Energy Lett.* **2021**, *6* (8), 2952−2959.

(8) Xu, Y.; Miao, R. K.; Edwards, J. P.; Liu, S.; O'Brien, C. P.; Gabardo, C. M.; Fan, M.; Huang, J. E.; Robb, A.; Sargent, E. H.; Sinton, D. A Microchanneled Solid Electrolyte for Carbon-Efficient CO_2 Electrolysis. *Joule* **2022**, *6* (6), 1333−1343.

(9) Kim, J. Y.; Zhu, P.; Chen, F.-Y.; Wu, Z.-Y.; Cullen, D. A.; Wang, H. Recovering Carbon Losses in CO_2 Electrolysis Using a Solid Electrolyte Reactor. *Nat. Catal.* **2022**, *5* (4), 288−299.

(10) Huang, J. E.; Li, F.; Ozden, A.; Rasouli, A. S.; Pelayo, F.; Arquer, G.; De; Liu, S.; Zhang, S.; Luo, M.; Xu, Y.; Bertens, K.; et al. CO_2 Electrolysis to Multi-Carbon Products in Strong Acid. *Science (80-.).* **2021**, *372*, 1074−1078.

(11) Al-Dhubhani, E.; Pärnamäe, R.; Post, J. W.; Saakes, M.; Tedesco, M. Performance of Five Commercial Bipolar Membranes under Forward and Reverse Bias Conditions for Acid-Base Flow Battery Applications. *J. Membr. Sci.* **2021**, *640*, No. 119748.

(12) Pärnamäe, R.; Mareev, S.; Nikonenko, V.; Melnikov, S.; Sheldeshov, N.; Zabolotskii, V.; Hamelers, H. V. M.; Tedesco, M. Bipolar Membranes: A Review on Principles, Latest Developments, and Applications. *J. Membr. Sci.* **2021**, *617*, No. 118538.

(13) Blommaert, M. A.; Aili, D.; Tufa, R. A.; Li, Q.; Smith, W. A.; Vermaas, D. A. Insights and Challenges for Applying Bipolar Membranes in Advanced Electrochemical Energy Systems. *ACS Energy Lett.* **2021**, *6*, 2539−2548.

(14) Holzapfel, P.; Bühler, M.; Van Pham, C.; Hegge, F.; Böhm, T.; McLaughlin, D.; Breitwieser, M.; Thiele, S. Directly Coated Membrane Electrode Assemblies for Proton Exchange Membrane Water Electrolysis. *Electrochem. Commun.* **2020**, *110*, No. 106640.

(15) Klingele, M.; Breitwieser, M.; Zengerle, R.; Thiele, S. Direct Deposition of Proton Exchange Membranes Enabling High Performance Hydrogen Fuel Cells. *J. Mater. Chem. A* **2015**, *3* (21), 11239−11245.

(16) Shafaque, H. W.; Lee, C.; Fahy, K. F.; Lee, J. K.; Lamanna, J. M.; Baltic, E.; Hussey, D. S.; Jacobson, D. L.; Bazylak, A. Boosting Membrane Hydration for High Current Densities in Membrane Electrode Assembly CO_2 Electrolysis. *ACS Appl. Mater. Interfaces* **2020**, *12* (49), 54585−54595.

(17) Ramdin, M.; Moultos, O. A.; van den Broeke, L. J. P.; Gonugunta, P.; Taheri, P.; Vlugt, T. J. H. Carbonation in Low-Temperature CO_2 Electrolyzers: Causes, Consequences, and Solutions. *Ind. Eng. Chem. Res.* **2023**, *62*, 6843−6864.

(18) Zhao, Y.; Hao, L.; Ozden, A.; Liu, S.; Miao, R. K.; Ou, P.; Alkayyali, T.; Zhang, S.; Ning, J.; Liang, Y.; Xu, Y.; Fan, M.; Chen, Y.; Huang, J. E.; Xie, K.; Zhang, J.; Brien, C. P. O.; Li, F.; Sargent, E. H.; Sinton, D. Conversion of CO_2 to Multicarbon Products in Strong Acid by Controlling the Catalyst Microenvironment. *Nat. Synth.* **2023**, *2*, 403−412.

(19) Peron, J.; Mani, A.; Zhao, X.; Edwards, D.; Adachi, M.; Soboleva, T.; Shi, Z.; Xie, Z.; Navessin, T.; Holdcroft, S. Properties of Nafion® NR-211 Membranes for PEMFCs. *J. Membr. Sci.* **2010**, *356* (1−2), 44−51.

(20) Stenina, I.; Golubenko, D.; Nikonenko, V.; Yaroslavtsev, A. Selectivity of Transport Processes in Ion-Exchange Membranes: Relationship with the Structure and Methods for Its Improvement. *Int. J. Mol. Sci.* **2020**, *21* (15), 5517.

(21) Balster, J.; Sumbharaju, R.; Srikantharajah, S.; Pünt, I.; Stamatialis, D. F.; Jordan, V.; Wessling, M. Asymmetric Bipolar Membrane: A Tool to Improve Product Purity. *J. Membr. Sci.* **2007**, *287* (2), 246−256.

(22) Luo, X.; Lau, G.; Tesfaye, M.; Arthurs, C. R.; Cordova, I.; Wang, C.; Yandrasits, M.; Kusoglu, A. Thickness Dependence of Proton-Exchange-Membrane Properties. *J. Electrochem. Soc.* **2021**, *168*, No. 104517.

(23) Bui, J. C.; Digdaya, I.; Xiang, C.; Bell, A. T.; Weber, A. Z. Understanding Multi-Ion Transport Mechanisms in Bipolar Membranes. *ACS Appl. Mater. Interfaces* **2020**, *12* (47), 52509−52526.

(24) Oener, S. Z.; Twight, L. P.; Lindquist, G. A.; Boettcher, S. W. Thin Cation-Exchange Layers Enable High-Current-Density Bipolar Membrane Electrolyzers via Improved Water Transport. *ACS Energy Lett.* **2021**, *6* (1), 1−8.

(25) Marcos-Madrazo, A.; Casado-Coterillo, C.; Irabien, Á. Sustainable Membrane-Coated Electrodes for CO_2 Electroreduction to Methanol in Alkaline Media. *ChemElectroChem.* **2019**, *6*, 5273−5282.

(26) Fischer, L.; Hartmann, S. S.; Maljusch, A.; Däschlein, C.; Prymak, O.; Ulbricht, M. The Influence of Anion-Exchange Membrane Nanostructure onto Ion Transport: Adjusting Membrane Performance through Fabrication Conditions. *J. Membr. Sci.* **2023**, *669*, No. 121306.

(27) Bühler, M. *Development of Novel Electrode Concepts for Proton Exchange Membrane Water Electrolyzers*; University of Freiburg: 2019.

(28) Lees, E. W.; Mowbray, B. A. W.; Salvatore, D. A.; Simpson, G. L.; Dvorak, D. J.; Ren, S.; Chau, J.; Milton, K. L.; Berlinguette, C. P. Linking Gas Diffusion Electrode Composition to CO_2 Reduction in a Flow Cell. *J. Mater. Chem. A* **2020**, *8* (37), 19493−19501.

(29) Zhang, N.; Liang, B.; Zhou, Y. H.; Wang, X. Y.; Kan, H. M.; Huang, W. X. Rheological Properties of SiC Suspensions with a Compound Surface Modification Using Ethyl Orthosilicate and Ethylene Glycol. *J. Dispers. Sci. Technol.* **2013**, *34* (12), 1742−1749.

https://doi.org/10.1021/acsenergylett.3c01716
ACS Energy Lett. 2023, 8, 4674−4683

(30) Vierrath, S.; Breitwieser, M.; Klingele, M.; Britton, B.; Holdcroft, S.; Zengerle, R.; Thiele, S. The Reasons for the High Power Density of Fuel Cells Fabricated with Directly Deposited Membranes. *J. Power Sources* **2016**, *326*, 170−175.
(31) Zabolotskii, V.; Sheldeshov, N.; Melnikov, S. Effect of Cation-Exchange Layer Thickness on Electrochemical and Transport Characteristics of Bipolar Membranes. *J. Appl. Electrochem.* **2013**, *43* (11), 1117−1129.
(32) Sacco, A. Electrochemical Impedance Spectroscopy as a Tool to Investigate the Electroreduction of Carbon Dioxide: A Short Review. *J. CO_2 Util.* **2018**, *27*, 22−31.
(33) Grew, K. N.; McClure, J. P.; Chu, D.; Kohl, P. A.; Ahlfield, J. M. Understanding Transport at the Acid-Alkaline Interface of Bipolar Membranes. *J. Electrochem. Soc.* **2016**, *163* (14), F1572−F1587.
(34) Yan, Z.; Mallouk, T. E. Bipolar Membranes for Ion Management in (Photo)Electrochemical Energy Conversion. *Accounts Mater. Res.* **2021**, *2* (12), 1156−1166.
(35) Ramírez, P.; Rapp, H. J.; Reichle, S.; Strathmann, H.; Mafé, S. Current-Voltage Curves of Bipolar Membranes. *J. Appl. Phys.* **1992**, *72*, 259−264.
(36) Chou, T.; Tanioka, A. Current-Voltage Curves of Composite Bipolar Membrane in Alcohol-Water Solutions. *J. Phys. Chem. B* **1998**, *102*, 7866−7870.
(37) Mayerhöfer, B.; McLaughlin, D.; Böhm, T.; Hegelheimer, M.; Seeberger, D.; Thiele, S. Bipolar Membrane Electrode Assemblies for Water Electrolysis. *ACS Appl. Energy Mater.* **2020**, *3* (10), 9635−9644.
(38) Grew, K. N.; Chiu, W. K. S. Stability & Kinetics of the Bipolar Membrane Interface: Implications for Electrochemical Technologies. *J. Electrochem. Soc.* **2020**, *167* (16), No. 164513.
(39) Xiao, Y. C.; Gabardo, C. M.; Liu, S.; Lee, G.; Zhao, Y.; O'Brien, C. P.; Miao, R. K.; Xu, Y.; Edwards, J. P.; Fan, M.; Huang, J. E.; Li, J.; Papangelakis, P.; Alkayyali, T.; Sedighian Rasouli, A.; Zhang, J.; Sargent, E. H.; Sinton, D. Direct Carbonate Electrolysis into Pure Syngas. *EES Catal.* **2023**, *1*, 54−61.
(40) Blommaert, M. A.; Sharifian, R.; Shah, N. U.; Nesbitt, N. T.; Smith, W. A.; Vermaas, D. A. Orientation of a Bipolar Membrane Determines the Dominant Ion and Carbonic Species Transport in Membrane Electrode Assemblies for CO_2 Reduction. *J. Mater. Chem. A* **2021**, *9* (18), 11179−11186.

https://doi.org/10.1021/acsenergylett.3c01716
ACS Energy Lett. 2023, 8, 4674−4683